Design study of a Magneto-Optical Trap for laser cooling of rubidium atoms.

Master's thesis
by
Erik Gustafsson

Lund Reports on Atomic Physics, LRAP-325
Lund, June 2004

Abstract

In this Master's thesis a Pyramidal Magneto-Optical Trap for rubidium has been designed. The trap is intended to be used in Atomic Physics courses for demonstration and laboratory exercises.

The theory for cooling and trapping ^{85}Rb and ^{87}Rb is developed. A detailed design of a low-cost and robust MOT is presented.

Two frequency locked laser systems have been built. Most of the components necessary to build the MOT have been identified, borrowed or purchased. The mechanical support to hold a pyramidal mirror has also been realized.

The report discusses how to complete the construction of the MOT.

Contents

Chapter 1

Introduction

In optical cooling, laser light is used to control the motion of atoms and slow them down. The average kinetic energy of a sample of atoms is often expressed as the corresponding temperature, $< E_k >= \frac{1}{2}k_BT$, in one dimension or $< E_k >= \frac{3}{2}k_BT$, if three dimensions are considered [4]. There are many different energy distributions with the same average energy. The subject of this Master's project, Doppler cooling, generates Bolzmann distributed atomic samples.

1.1 Research

Cooling and trapping of atoms is one of the largest contemporary research areas in atomic physics.

The development of narrow band tunable lasers has made it possible to control the movement of atoms, with high precision. S Chu, C Cohen-Tannoudji and W D. Phillips received the Nobel price in 1997 for their development of cooling and trapping techniques. The most famous application of cooling and trapping is Bose Einstein Condensation (BEC). When a number of atoms move slowly enough and come close enough to one another, they will all condensate into the lowest energy level. Bose and Einstein presented the theory of BEC in 1923. In 1995 E. A. Cornell, W. Ketterle and C. E. Wieman managed to reach BEC. In 2001 they received the Nobel price for their work.

Cold atoms is an active research area also in Scandinavia. There are experimental groups in Umeå, Copenhagen and Aarhus.

1.2 The project

The goal of this master's project was to construct equipment for a laboratory exercise about cold atoms. The laboratory exercise is planned to be a part of

the atomic physics education at Lund Institute of Technology. Developing the laboratory exercise is a part of the project.

The first aim for the project was to achieve Optical Molasses, that is to cool but not trap atoms. Diode lasers used for Rubidium spectroscopy were planned to be used. After some studying of literature and articles in the subject and correspondence with Anders Kastberg, University of Umeå, we decided to start planning and building a Magneto Optical Trap (MOT). In a MOT atoms are both cooled and trapped, which results in denser clouds of slowly moving atoms.

Rubidium was chosen to be cooled mainly because there were diode lasers available. It later turned out that diode lasers have to be placed in an external cavity in order to be able to lock their frequency to an atomic transition. The available lasers did not have any external cavity. To solve this problem two external cavity diode lasers were built. A MOT based on a pyramidal geometry was designed and most of its components purchased. A laboratory exercise using the laser system for saturation spectroscopy was also developed and given to the students of the Advanced Atomic Physics Course.

Chapter 2

Cooling and trapping rubidium

2.1 Rubidium, an alkali-metal

Rubidium is an Alkali-metal. The Alkali-metals were the first group of atoms that was cooled and trapped [1]. They have transitions from the ground state to excited states, that correspond to wavelengths in the visible or near infra red (NIR) regions. They can also easily be generated in atomic beams. These two properties make them very suitable for cold atom experiments.

Natural rubidium contains two isotopes ^{85}Rb (72 %) and ^{87}Rb (28 %). The two isotopes have different nuclear spin, which leads to different hyperfine splittings, shown in figure 2.1. The first transitions from the ground state are called D1 and D2. The hyperfine splittings of these lines are exaggerated in the figure.

The theory of optical cooling is evaluated from two level systems. In multilevel systems such as Rubidium it is necessary to find a closed transition, where only two energy levels participate. Atoms that are in the exited state of the transition will according to the selection rules only be able to deexite to the ground state of the transition. The closed transitions that are used for cooling ^{85}Rb and ^{87}Rb are drawn in figure 2.1.

In a Magneto Optical Trap the atoms are moving in an inhomogeneous magnetic field. The laser light that is used is circularly polarized light (σ^+ and σ^-). In figure 2.2 the splittings of the cooling transitions are pictured, for a magnetic field B$<$0. The transition that are shown are valid for σ^+-light. ^{85}Rb atoms that scatter σ^+ will be optically pumped towards M_F=3 in the ground state and ^{87}Rb will be pumped towards M_F=2. Atoms that mainly absorb σ^- are pumped towards M_F=-3, ^{85}Rb and M_F=-2, ^{87}Rb. This means that it is still possible to approximate the transitions with two level schemes.

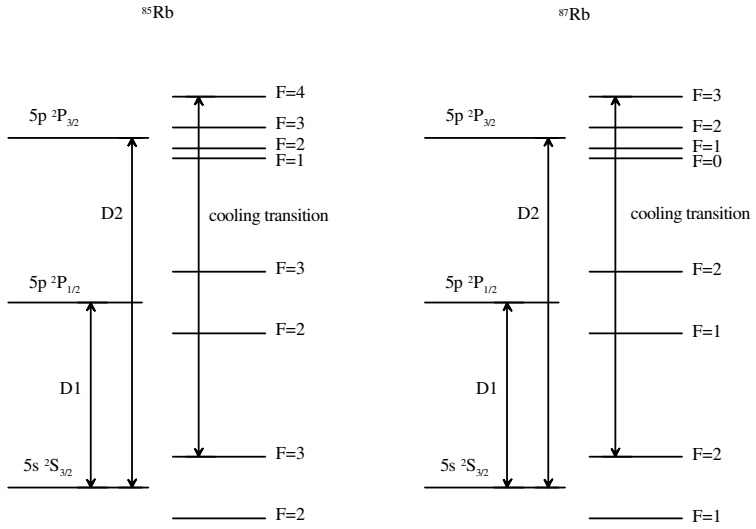

Figure 2.1: Energy levels of the two rubidium isotopes. λ_{D1}=795 nm , λ_{D2}=780 nm

2.1.1 Atomic data for ^{87}Rb

Property	Symbol	Value	
atomic mass	M	86,909 u	
nuclear spin	I	3/2	
wavelength of the D2 line in vacuum	λ	780,241 nm	
wavelength of the D2 line in air	λ_{air}	780,032 nm	[1] [20]
natural line width	Γ	6,065 MHz	
saturation intensity	I_0	1,6 mW/cm^2	
Landé factor, ground state, D2	g_a	1/2	
Landé factor excited state, D2	g_b	2/3	

2.2 Rubidium in an electromagnetic laser field

2.2.1 Light pressure

When rubidium atoms are irradiated by light with a wavelength of ∼780 nm that corresponds to the cooling transition in one of the isotopes, three processes take place. Absorption of a photon (W_{ab}) can occur. The exited atoms can return to the ground state by spontaneous emission (Γ) or stimulated emission (W_{ba}). Figure 2.3 shows these processes for the two rubidium isotopes. The

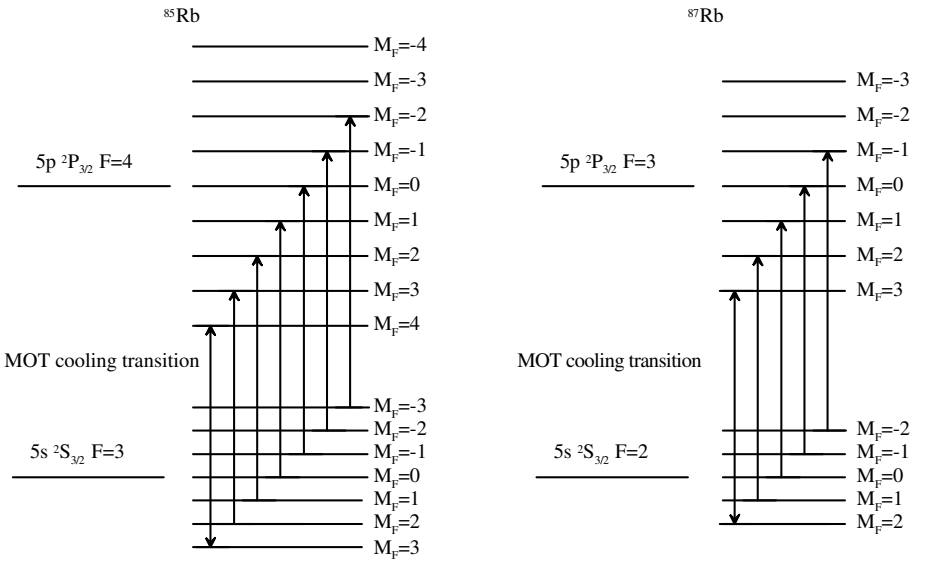

Figure 2.2: Magnetic sub levels of the cooling transitions from figure 2.1. B<0

rate equations for the evaluation of the populations can be written as:

$$\frac{dN_a}{dt} = \Gamma N_b + W_{ba}N_b - W_{ab}N_a \tag{2.1}$$

$$\frac{dN_b}{dt} = -\Gamma N_b - W_{ba}N_b + W_{ab}N_a \tag{2.2}$$

A steady state solution of the rate equations gives the fraction of excited atoms.

$$\frac{N_b}{N_t} = \frac{W/\Gamma}{1 + 2W/\Gamma} \tag{2.3}$$

The expression can be rewritten by introducing the absorption cross section, σ.

$$W = \sigma\phi \tag{2.4}$$

ϕ is the photon flux

Due to the limited lifetime of the excited state, the cross section can be expressed as [2]:

$$\sigma(\omega) = \frac{\sigma_0}{1 + (\frac{2\delta_l}{\gamma})^2} \tag{2.5}$$

$\sigma_0 = \sigma(\omega_{ba})$, $\delta_l = \omega - \omega_{ba}$, ω is the laser frequency, ω_{ba} is the resonance frequency of the cooling transition and $\gamma = 2\pi\Gamma$ is the natural line width.

Inserting equation 2.4 and 2.5 into equation 2.3 results in:

$$\frac{N_b}{N_t} = \frac{1}{2}\frac{I/I_0}{1 + (\frac{2\delta_l}{\gamma})^2 + I/I_0} \tag{2.6}$$

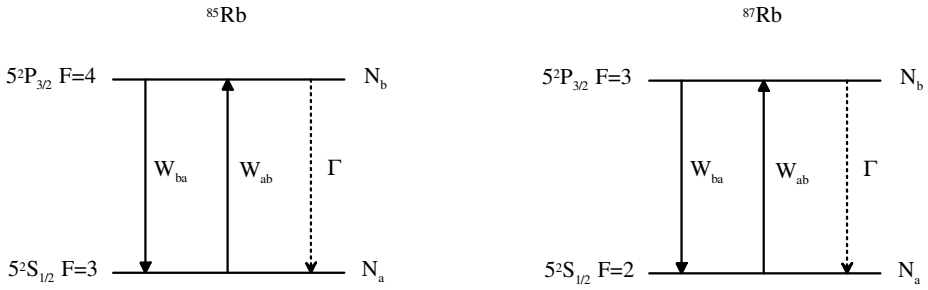

Figure 2.3: The coupling between the ground states and the excited states. $W_{ab} = W_{ba} = W \quad , \quad N_t = N_a + N_b$

To simplify the expression the saturation intensity $I_0 = \frac{\hbar\omega\Gamma}{2\sigma_0}$ was introduced.

The fraction of excited atoms gives the scattering rate, R and the average force that the light exerts on each atom. The momentum kicks from the spontaneous emission are in random directions, they do not contribute to the average force.

$$\vec{F} = R\vec{p}_{photon} = \frac{N_b}{N_t}\Gamma\hbar\vec{k}_{photon} = \frac{1}{2}\frac{I/I_0}{1+(\frac{2\delta_l}{\gamma})^2 + I/I_0}\Gamma\hbar\vec{k}_{photon} \tag{2.7}$$

2.2.2 Slowing rubidium atoms in motion

If the atoms are in motion, the Doppler shift has to be taken into consideration:

$$\delta_d = -\vec{k}\cdot\vec{v}_{atom} \tag{2.8}$$

The force as a function of the atom velocity can be calculated by just adding the Doppler shift to the laser shift in the expression, that was evaluated in the previous section.

By using two laser beams directed in opposite direction with overlapping beam paths, a friction force in one dimension is created.

$$\vec{F} = \frac{1}{2}\left(\frac{I/I_0}{1+(\frac{2(\delta_l-\vec{k}\cdot\vec{v}_{atom})}{\gamma})^2 + I/I_0} - \frac{I/I_0}{1+(\frac{2(\delta_l+\vec{k}\cdot\vec{v}_{atom})}{\gamma})^2 + I/I_0}\right)\Gamma\hbar\vec{k}_{photon} \tag{2.9}$$

The force on ^{87}Rb atoms is plotted for various laser detunings in figure 2.4. The rubidium data are listed in section 2.1.1. The laser beam is assumed to have a power of 10 mW and a Gaussian beam profile with a diameter of 30 mm.

The plotted force is the average velocity dependent force. It can be seen in the figure that a small detuning gives a force with a small magnitude. A large detuning gives a force with a large maximum value but it decreases for small atomic speeds. The detuning that slows the atoms to the lowest theoretical value is $\delta_l = -\gamma/2$. See section 2.3 for a more detailed discussion.

The setup can be expanded to three dimensions with three pairs of laser beams. The slow moving cloud of atoms that is created in such a setup is often called

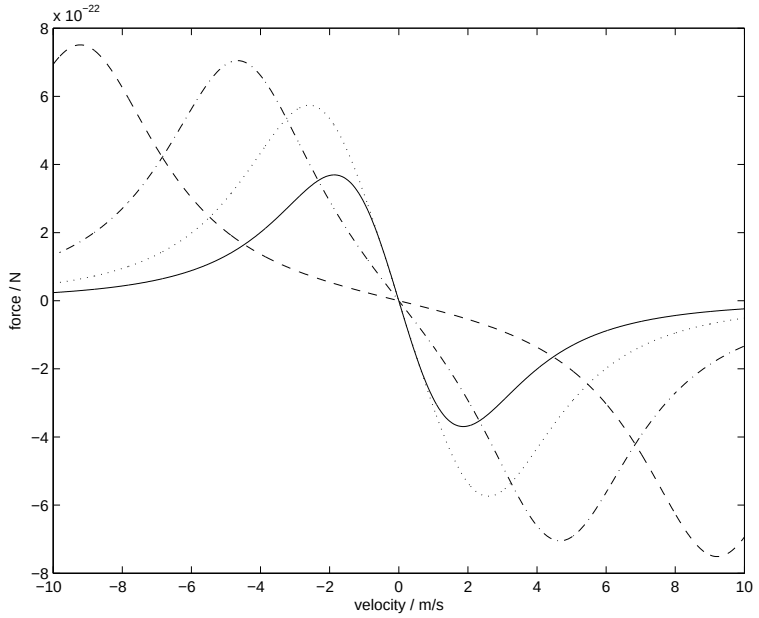

Figure 2.4: The average force acting on a ^{87}Rb atom as a function of the velocity of the atom. Laser detuning $\delta_l = -\frac{\gamma}{4}$, solid line; $\delta_l = -\frac{\gamma}{2}$, dotted line; $\delta_l = -\gamma$, dash-dotted line and $\delta_l = -2\gamma$, dashed line.

optical molasses. There is nothing that keeps the atoms within the cloud. They move slowly but are not trapped.

2.2.3 Restoring force

To trap atoms a position dependent force that pushes atoms towards a certain point is needed. As mentioned in section 2.1, in the Magneto Optical Trap this is ensured by applying an inhomogeneous magnetic field and using circularly polarized laser light.

The inhomogeneous magnetic field is usually created by two coils in anti-Helmholtz configuration, see section 3.8. In one dimension the magnetic field can be written as:

$$B(z) = Az \tag{2.10}$$

The Zeeman shifts of the levels participating in the MOT cooling transition [3], figure 2.2, give rise to a position dependent frequency shift of the cooling transition.

$$\delta_{\pm}(z) = -\frac{(g_b M_b - g_a M_a)\mu_B A z}{\hbar} \tag{2.11}$$

δ_+ is the frequency shift of the transition that is driven by σ^+ light and δ_- is the shift for the transition driven by σ^-. g_a and g_b are the Landé factors for the ground state and the excited state of the transitions. M_a and M_b are the

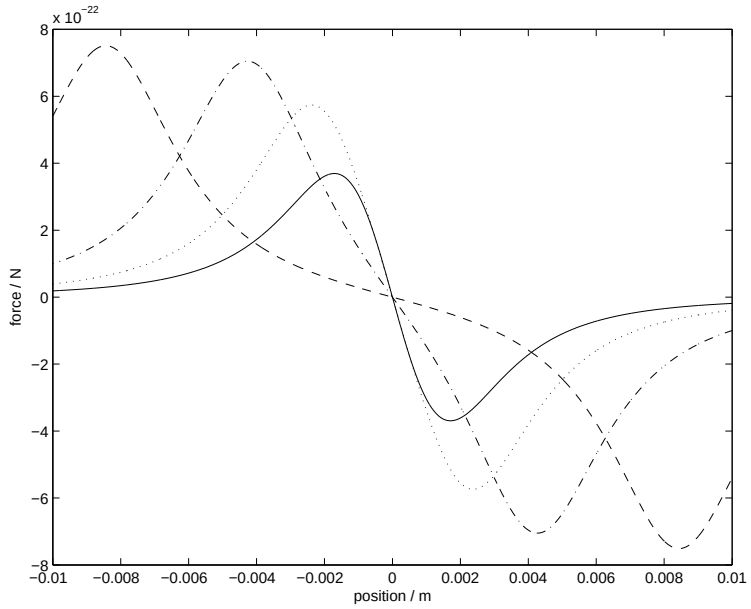

Figure 2.5: The average position dependent force in a MOT for ^{87}Rb. Laser detuning $\delta_l = -\frac{\gamma}{4}$, solid line; $\delta_l = -\frac{\gamma}{2}$, dotted line; $\delta_l = -\gamma$, dash-dotted line and $\delta_l = -2\gamma$, dashed line.

magnetic quantum numbers of the two states participating. In the transition excited by σ^+, M_a=3 and M_b=4 in ^{85}Rb and M_a=2 and M_b=3 in ^{87}Rb. In the transitions excited by σ^- the magnetic quantum numbers are of the same value but negative.

A restoring force in one dimension can be achieved by having two counter propagating laser beams just like in section 2.2.2. The beam with a positive k-vector has σ^+ polarization and the beam with negative k-vector is σ^- polarized. In this arrangement both a position dependent trapping force and a slowing friction force is achieved.

$$\vec{F} = \frac{1}{2}\left(\frac{I/I_0}{1+\left(\frac{2(\delta_l-\vec{k}\cdot\vec{v}_{atom}+\delta_+(z))}{\gamma}\right)^2+I/I_0} - \frac{I/I_0}{1+\left(\frac{2(\delta_l+\vec{k}\cdot\vec{v}_{atom}+\delta_-(z))}{\gamma}\right)^2+I/I_0}\right)\Gamma\hbar\vec{k}_{photon} \tag{2.12}$$

To cool and trap in three dimensions it takes three pairs of σ^+- and σ^--beams and a magnetic field that has linear dependence in three dimensions.

The force as a function of z, v=0 is plotted in figure 2.5. The plot is done for some different detunings. From the plot it can be seen that the detuning affects the size and the density of the cloud of trapped atoms.

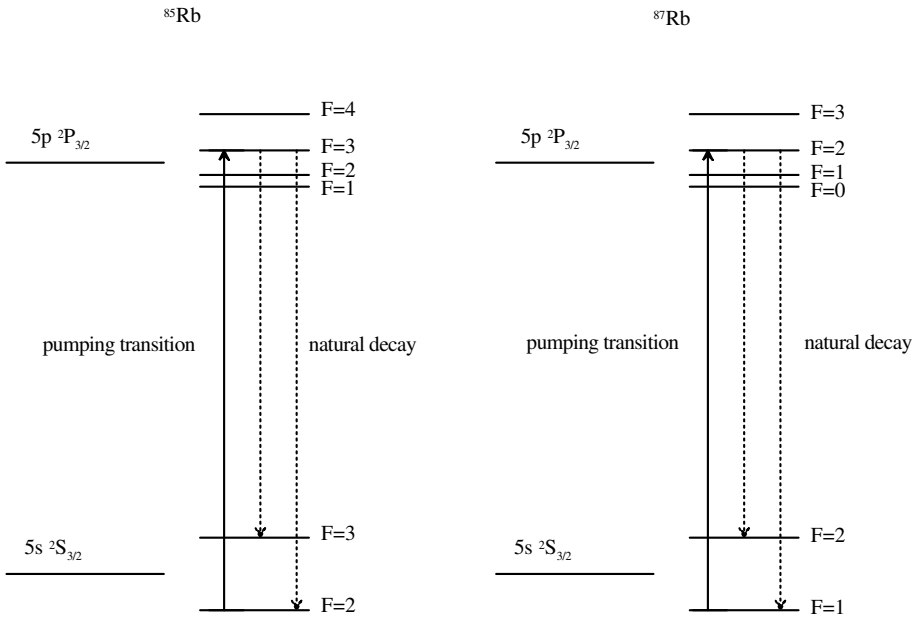

Figure 2.6: Hyperfine pumping to the excited states F=3 in ^{85}Rb and F=2 in ^{87}Rb.

2.2.4 Hyperfine pumping

When rubidium atoms scatter photons at the cooling transition, they make a forbidden transition about 1/1000 [9] of the deexcitations and end up in F=2, ^{85}Rb or F=1, ^{87}Rb. In these states the atoms can not be further cooled. They have to be excited from, F=2 (ground state) to F=2 or 3 (excited state), if ^{85}Rb is cooled or from, F=1 (ground state) to F=1 or 2 (excited state), in ^{87}Rb. The atoms can then deexcite to the F=3, ^{85}Rb or F=2, ^{87}Rb spontaneously. The hyper fine pumping schemes are shown in figure 2.6. The pumping is very quick and is practically achieved by using another laser with a the frequency that matches one of the transitions described above.

2.3 Cooling limits

2.3.1 Capture limit

Atoms moving with a speed which makes them just at the boundary of absorbing light and thus slowed down are at the capture limit.

In figure 2.4 it can be seen that the friction force increases when the speed of the atoms increase, but for atom speeds that correspond to a Doppler shift that is larger than the detuning, the force is decreasing again. This means that atoms

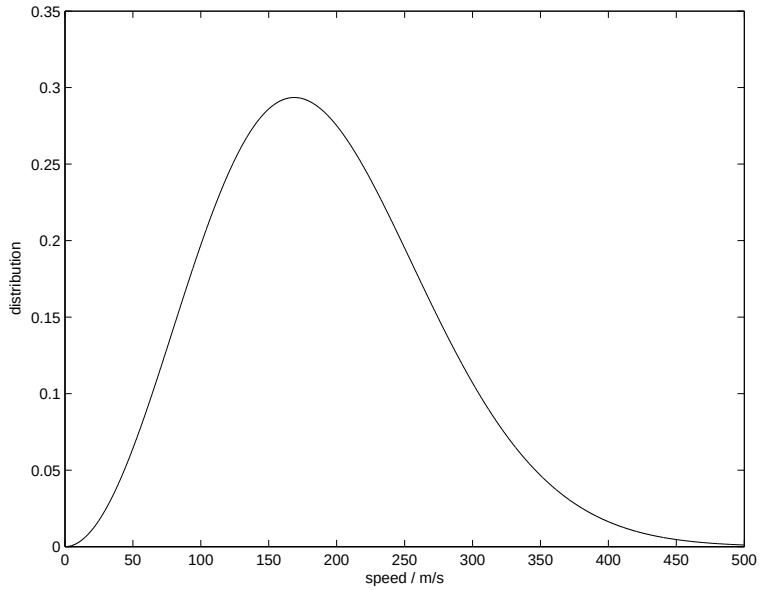

Figure 2.7: The speed distribution of rubidium atoms at T=293 K.

with large speeds will not be cooled.

The capture limit is dependent on the detuning. A large detuning makes it possible to cool many atoms, but on the other hand they will not move as slowly as possible. The detuning that creates the coldest sample is $\delta_l = -\gamma/2$. For this detuning the capture limit is defined as [1]:

$$v_c k \equiv \gamma \tag{2.13}$$

Sometimes it is handy to express the capture limit as a temperature.

$$k_B T_c \equiv \frac{M\gamma^2}{k^2} \tag{2.14}$$

M is the atomic mass. For ^{87}Rb the capture limit is 4,6 m/s or 0,22 K.

A common way of loading a MOT is to catch atoms from the background vapor. In the design described in this report, that method will be used to load the trap with one of the Rubidium isotopes. The capture limit is approximately valid for a MOT, although there is a position dependent frequency shift in addition to the Doppler shift. There is just a tiny fraction of the atoms that move slower than the capture limit if the atoms are at thermodynamic equilibrium at room temperature. At thermodynamic equilibrium atoms are Maxwell-Bolzmann distributed, equation 2.15 [4]. Equation 2.15 is plotted for Rb^{87} at room temperature in figure 2.7.

$$f(v) = \frac{4}{\sqrt{\pi}}(\frac{M}{2k_B T})^{3/2} v^2 e^{\frac{mv^2}{2k_B T}} \tag{2.15}$$

In ^{87}Rb about 15 atoms out of 100000 move below the capture limit. The detuning can be increased in order to catch a larger fraction of the atoms.

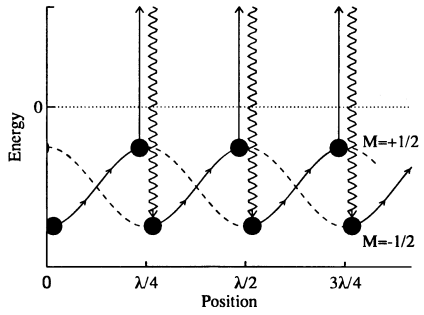

Figure 2.8: The light shift and transitions of Sisyphus cooling.[1]

2.3.2 Doppler limit

In figure 2.4 the average force is plotted. If this force alone was controlling the motion of the atoms, all of the atoms below the capture limit would be cooled down to zero speed. There are however other effects that have to be taken into consideration. The cause of the average force is many momentum kicks when the atom absorbs photons. Depending on the speed of the atom there is a probability of absorbing a photon from either one of the lasers. The spontaneous emission is in random directions. These two effect causes a Brownian motion in the phase space for the atom [1]. At steady state the cooled atoms have a characteristic speed that corresponds to a temperature of:

$$k_B T_d = \frac{\hbar\gamma}{2} \tag{2.16}$$

This temperature is usually called the Doppler limit. It is reached when the laser detuning is $\gamma/2$. It is reasonable that this detuning gives rise to the coldest samples. If the detuning is larger, atoms with a speed that is close to zero will sense a reduced average force, see figure 2.4. A detuning that is smaller than $\gamma/2$ causes an increased absorption from both lasers for atoms with almost zero speed. These absorptions cause heating.

The value of the Doppler limit does not differ much between the two isotopes, v_d=12 cm/s and $T_d = 140\mu K$, is valid for both [1].

It was thought to be lowest reachable temperature with optical cooling schemes. But Sisyphus cooling and $\sigma^+ - \sigma^-$-cooling can take part in optical cooling schemes and lower the temperature a bit further.

Sisyphus-cooling relies on light shifts in a standing wave with polarization gradients and optical pumping among the magnetic sub levels. Sisyphus-cooling can be obtained in one dimension by having two counter propagating linearly polarized beams with perpendicular polarization directions. The standing wave pattern in such a configuration changes polarization from linearly polarized through σ^+, linearly polarized (out of phase), σ^- then again linearly polarized with the same phase as in the starting point. In atoms like Rb with multiple

magnetic sub levels in the ground state, optical pumping processes tends to redistribute the population. Rubidium is pumped towards M_a=3, ^{85}Rb and M_a=2, (^{87}Rb) in places where the polarization is σ_+ and the corresponding negative values where the polarization is σ_-. These optical pumping processes take a finite time. For red detuned light the light shift is negative for the ground state and the atoms tend to be pumped towards the sub states with the lowest energy. Atoms in motion will always move uphill energy wise and be further cooled, figure 2.8[8].

As the name reveals $\sigma^+ - \sigma^-$-cooling uses two counter propagating circularly polarized beams. The resulting standing wave is linearly polarized with a polarization direction that rotates 2π over a wavelength. Linearly polarized light tends to pump atoms towards M_a=0. When atoms are moving in a field with rotating polarization the atoms atoms will not be pumped quickly enough and thereby lag after the distribution of a an atoms that is standing still in the same position. For Rubidium the result is that atoms moving towards the σ^+ tends to be pumped towards M_a=3, ^{85}Rb and M_a=2, (^{87}Rb). Atoms in these sub states has a much higher probability of absorbing a σ^+-photon than a σ^--photon, due to the Clebsch-Gordan coefficients. The damping force is increased. The same arguments hold for atoms moving towards the σ^--beam [1].

In a three dimensional MOT there will be polarization gradients and the temperature can reach below the doppler limit. Temperatures around 1μK have been measured [9]

2.3.3 Recoil limit

The lowest temperature that can be approached with any kind of optical cooling scheme is the recoil limit, that is the atomic speed and temperature that corresponds to the momentum of a single photon. It takes other non optical mechanisms to go beyond this limit. To get close to the recoil limit is beyond the aim of this MOT design. The recoil limit in rubidium is v_r=0,6 cm/s, which corresponds to a temperature of $T_r = 0,4\mu$K.

Chapter 3

MOT design

The aim for this MOT project, is to design a trap that is reliable, easy to setup and affordable. The pyramidal MOT fulfils all of the criterions.

In a pyramidal MOT the three pairs of σ^+- and σ^--beams that are needed for cooling and trapping in three dimensions are created by letting an expanded σ^-- (or σ^+-) beam get reflected in a hollow pyramid, figure 3.1.

To understand how the circular polarization changes when the expanded beam gets reflected in the hollow pyramid, it is easier to see the expanded beam as a large number of narrow beams. Before hitting the first mirror the partial beams are right circularly polarized, with their direction of propagation as a reference. When getting reflected in the first mirror the polarization changes to left circularly polarized, in the same reference system. The reflection in the second mirror changes the polarization once more and the partial beam is right circularly polarized again but in a reference direction that points in opposite direction compared to before the reflections. Three pairs of counter propagating beams, where each beam pair have the same polarization, when having their direction of propagation as a reference is what is needed in a MOT.

The design was developed by Lee *et al* [7]. This type of MOT reduces the number of optical components and thus the costs. The disadvantage with the pyramidal MOT is mainly the reduced optical access.

3.1 Setup

The optical layout can be seen in figure 3.2.

A small fraction (10%) of the light from the lasers is split off to use in the saturation spectroscopy setup. The rest of the beams are shaped, expanded and made circularly polarized before entering the chamber. Behind the view port of the chamber is the hollow pyramid placed, where the Rb atoms are cooled and trapped.

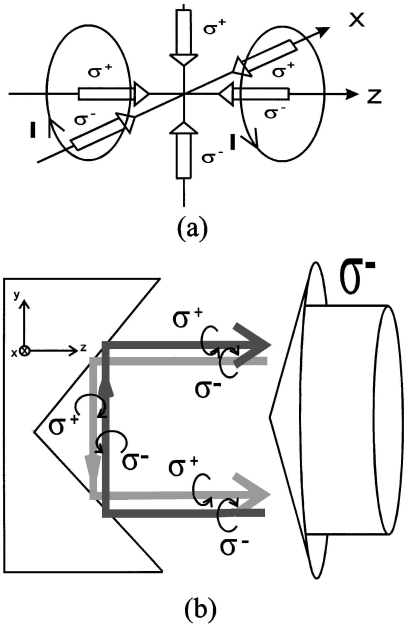

Figure 3.1: (a) The circularly polarized beams and the coils of a conventional MOT. (b) The partial beams of a pyramidal MOT.[7]

Diode lasers tend to have an elliptical beam profile. The beam shaping is done to make the beam profile more circular by letting the beam trough either an anamorphic prism pair or a polarization preserving single mode optical fibre. The beam shaping might not be needed if the long axis of the elliptical profile is adjusted to be parallel with one of the reflecting surfaces of the pyramidal mirror. If this is done the elliptical beam profile will not cause disturbances in the force balance.

The saturation spectroscopy setup is used to get a Doppler free spectra from rubidium. The lasers will be locked to the peaks in the spectrum that corresponds to the cooling transition and the hyperfine pumping transition.

3.1.1 The chamber

The design of this chamber is based on an article by A. S. Mellish and A. C. Andrews [10]. A five way vacuum cross of ISO-KF standard will be used as the chamber. The cross has an inner diameter of 40,4 mm. The distance between two facing openings is 130 mm. One of the openings will just be used to set the cross on an optical table. In the other four entrances there will be attached, one or two vacuum pumps, an electrical feedthrough with a Rubidium dispenser and a view port behind which a pyramidal mirror will be placed, see figure 3.2.

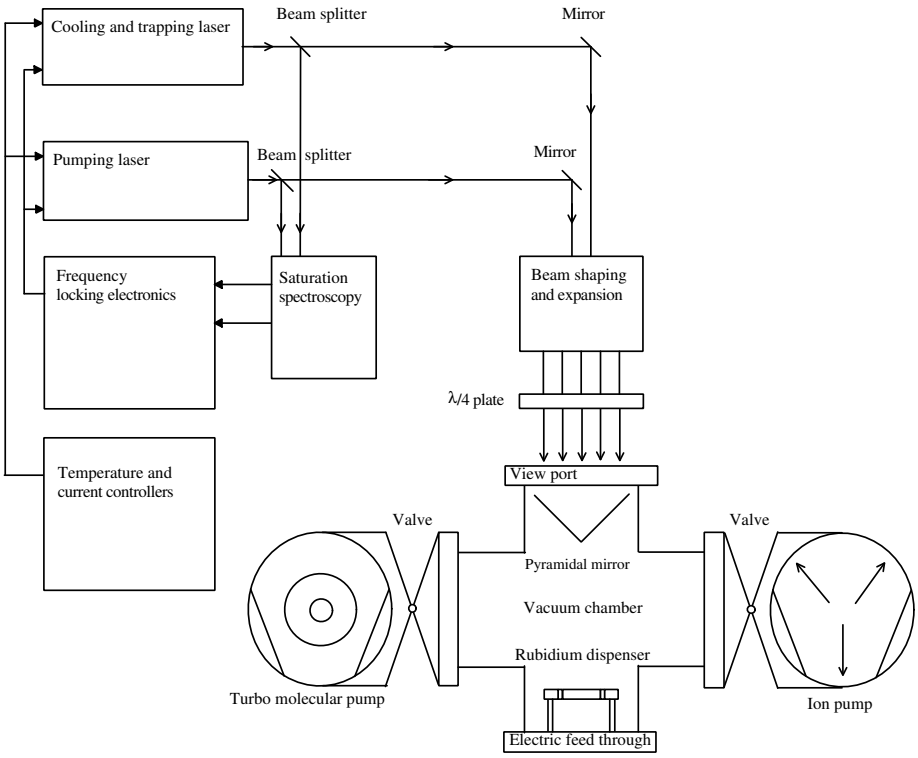

Figure 3.2: Optical layout and trapping chamber

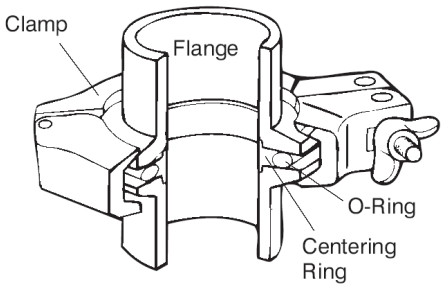

Figure 3.3: ISO-KF vacuum standard

Vacuum and Rubidium pressure

It is possible to run a MOT at a pressure of about 10^{-5} Pa, but the lifetime of the atoms in the MOT is short and it is hard to perform any interesting measurements. At a pressure of 10^{-6}-10^{-7} Pa the lifetime is sufficient for most experiments [9]. At higher rubidium pressure the fluorescence from the background gas makes the trap difficult to see.

It is usually recommended to build the chamber with components of Conflat type [10]. In this standard each vacuum pipe ends with a flange that is bolted to another flange and sealed with copper gaskets. To reduce costs the chamber will be constructed with ISO-KF components instead. In this standard the sealing between pipe ends is ensured by a clamping ring and an o-ring, figure 3.3. Even if the best o-rings are chosen (Viton), outgassing from the o-rings might be a problem when trying to reach low enough pressure.

To pump the system down to the required pressure a portable turbo molecular pump will be used, Edward EXT70. This pump has a pumping capacity of 50 ls^{-1} and is specified to pump down to an ultimate pressure below $5{\cdot}10^{-7}$ Pa. If this pump is not good enough, or if it is not available after the system has been pumped down, an Ion pump can be attached to the chamber. Vacuum pumps with a capacity of 2 l/s have been used in similar chambers [10], but a pump capacity of $\sim$10 l/s is probably a better choice.

The vacuum pumps will be connected to the chamber via vacuum valves. There are VAT vacuum gate valves available. These valves are not all metal valves and outgassing might be a problem. If they do not work sufficiently well, the pumps can be connected without any valves or with all metal ones.

The amount of Rubidium in the chamber can be regulated with a Rubidium dispenser. The dispensers are bought from Saesgetters. The material that generates Rubidium is a mixture of Rubidium chromate (Rb_2CrO_4) and a reducing agent. The reducing agent acts as an electron donor, when it reacts with the Rubidium chromate free Rubidium atoms are produced. The rate in which free rubidium is produced can be controlled by letting a current through the dispenser.

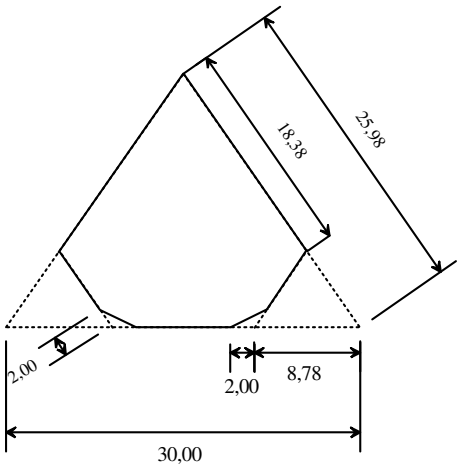

Figure 3.4: Four glass pieces of this shape forms a hollow pyramid. The top angle is 70,53 ° All lengths in mm

The dispenser is shaped as a bar with an overall length of 32 mm. In each end of the bar is a 10 mm long electrical terminal, where a voltage can be applied. The active region where rubidium is set free is the 12 mm at the center of the bar. According to the manufacturer, the rubidium evaporation starts when a current of 5,3 A is led through the dispenser, at this current the dispenser has a temperature of about 850 K [11]. This current is probably not needed to produce the small amounts of rubidium that are required to operate the trap. Much of the rubidium will stick to the walls, but the getter can evaporate enough rubidium to compensate for this pump effect. Wieman *et al* has ran a similar Rb-MOT for more than 100 h without any depletion of the getter [9].

The dispenser contains 4,5 mg Rubidium with the natural contribution between the isotopes (72 % ^{85}Rb and 28% ^{87}Rb). The current to the dispenser is led through an electrical vacuum feed through. A constant current generator to provide a stable current through the dispenser has to be purchased or constructed.

Pyramidal mirror

The design of the pyramidal mirror is slightly modified from the design described by Wilson *et al* [10]. The modifications were made to make the mirror fit better in the vacuum crossing that is planned to be used as a chamber. To be able to place the mirror as close as possible to the view port, the spacing in between the pyramidal mirror and the walls of the vacuum crossings is increased in this design. The enlarged spacing ensures that Rubidium can diffuse into the hollow pyramid even if it is placed a little closer to the view port than the 16 mm, which was the spacing Wilson *et al* used [10].

To form a pyramid with a 90 degree top angle between facing sides, each side must be a triangle with the proportions $(1 : \sqrt{3}/2 : \sqrt{3}/2)$. The pyramidal mir-

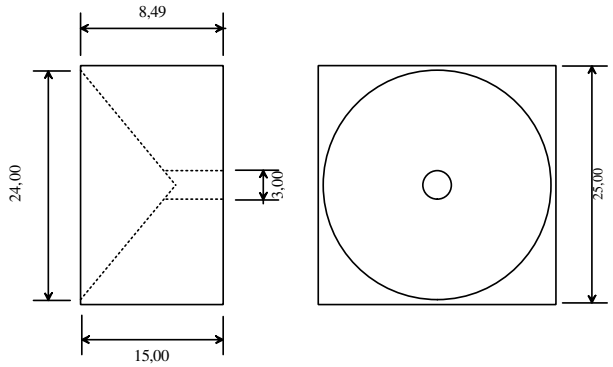

Figure 3.5: Stainless steel block with a machined hollow cone, in which the glass pieces that form the hollow pyramid will be mounted.

ror is manufactured out of four triangular glass pieces. To make the pyramidal mirror fit in a vacuum pipe, two edges of the glass pieces are cut off, see figure 3.4. The glass pieces will be coated with silver before they are glued in a hollow cone which base diameter and hight has a ratio of 1:$\frac{1}{2\sqrt{2}}$. Low vapor pressure epoxy is a suitable glue. The hollow cone has been machined into a stainless steel block, figure 3.5.

Gold has a higher reflectivity at 780 nm than silver, but gold tends to attract rubidium to stick upon it, with a reduced reflectivity as a consequence. Dielectric mirrors can be made with higher reflectivity than metal mirrors but in general they are not polarization preservable.

Generation of the magnetic field

To generate a magnetic field with an approximately linear dependence in all three dimensions coils in an anti Helmholtz configuration are used, figure 3.6. The magnetic fields of the two coils are set to counteract by letting a current flow trough the coils in opposite directions.

The magnitude of the magnetic field from a single coil at a distance z from the coil is:

$$B = \frac{\mu_0 I r^2}{2(r^2 + z^2)^{3/2}} \tag{3.1}$$

See figure 3.7 for an explanation of the notations.

The magnetic field for two multiple turn coils in anti Helmholtz configuration can be calculated by summing the field from many single coils. A magnetic field gradient of 0,20 T/m gives a sufficient restoring force [9]

In figure 3.8 the magnetic field for some different spacings between the two coils are plotted, it can be seen that when the spacing equals the radius of the coils, the biggest magnetic field gradient is accomplished. The calculations are done

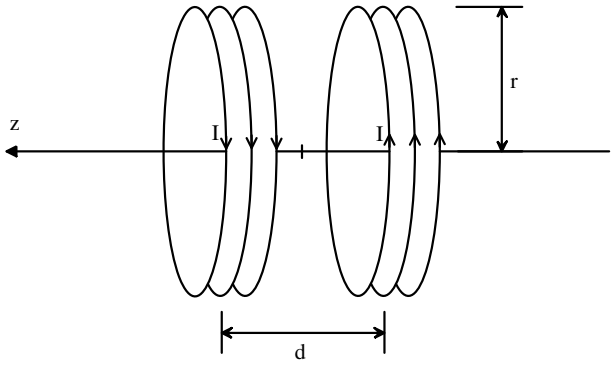

Figure 3.6: Two coils in anti-Helmholtz configuration

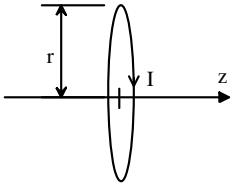

Figure 3.7: A single coil.

for 28 mm average radius of the coils, which means that the coils can be wound on the outside of the chamber. With a total integrated current of 300 A through the cross section of the coils (10mm×10mm) a magnetic field gradient of 0.20 T/m is achieved. If choosing copper wire with a diameter of 1 mm at least 100 turns of wire will fit within the cross section. The current through each single coil will then be 3 A.

There will be a temperature increase in the coils due to their resistance. If the temperature increases at the most 30°, the resistance of the coils will be less than 0.5 Ohm each. The heating power of each coil is then smaller than 4.5 Watts. The heating power depends on the cross section of the coils. It is independent of if a thick wire with a few turns and a high current is used, or if a thin wire with many turns and a small current is used.

It takes 3 volts to run a current of 3 A through the coils. This is reasonable values for a constant current power supply. A power supply that cover these demands is being manufactured in the electronics workshop.

The restoring force of the MOT is directed towards the point where the magnetic field is zero. The earth magnetic field and stray field from ion pumps will shift the position of zero magnetic field from the center in between the coils. In a pyramidal MOT this is not a problem. It is actually undesirable to have the MOT in the center of the pyramid, because of scattering of the reflected light in the intersections between the mirrors. But the point were the field is zero must be within the hollow pyramid. To ensure this it might be necessary to put

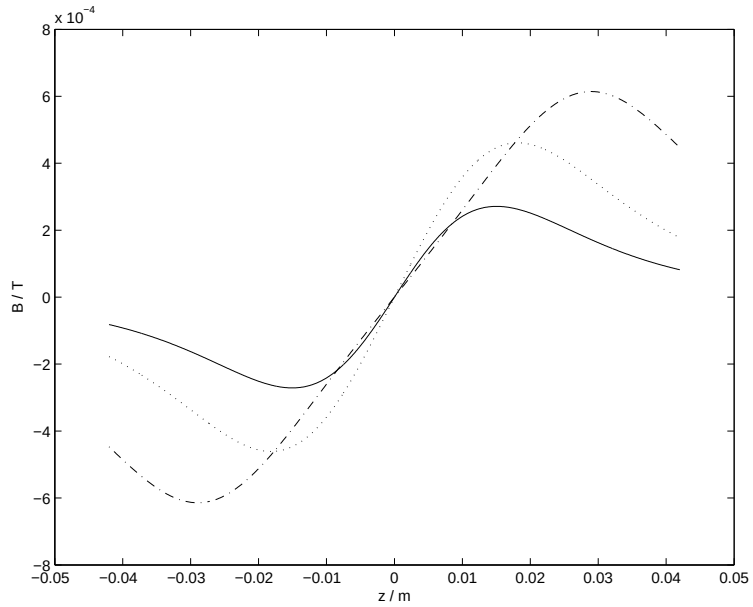

Figure 3.8: Magnetic field from two coils in anti-Helmholtz configuration. Solid line for a spacing of d=r/2, dotted line d=r and dash-dotted line d=2r.

the stainless steel block on spacers, move the coils or have an additional small compensating coils system.

3.1.2 Saturation spectroscopy

The first experiments that were carried out during this project was saturation spectroscopy of rubidium. The obtained spectra initially seemed very simple to interpret. There are however cross over peaks and hyperfine pumping effects that makes the interpretation a little complex.

In the laboratory exercise that was given in the Advanced Atomic Physics course the students built a saturation spectroscopy setup to receive a doppler free signal.

In figure 3.2 it can be seen that about 10 % of the two laser beams are split off to the saturation spectroscopy setup. The two beams are led through a rubidium cell. These high power beams act as pump beams. The pump beams gets reflected in a couple of neutral density filters to create two probe beams that are sent back through the cell. The pump and probe beams must intersect in an angle that is as narrow as possible. After the rubidium cell the probe beam hits a photodiode. The signal from the photodiode is led to the frequency locking lock in amplifier.

In the doppler broadened spectra at room temperature, the D2 line consists of

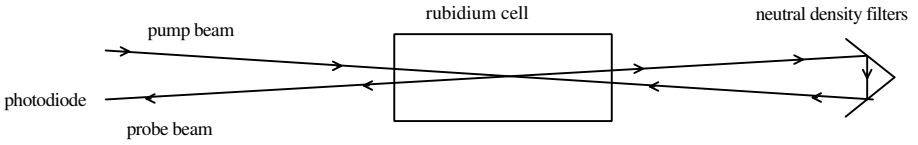

Figure 3.9: Optical layout for a saturation spectroscopy setup.

two peaks. The doppler broadening is smaller than the hyperfine splitting in the ground state but larger than the splitting of the excited state. The two peaks are 3 GHz apart in ^{85}Rb and separated by 7 GHz in ^{85}Rb.

The theory of saturation spectroscopy can be found in for instance [17]. Saturation spectroscopy can resolve the hyperfine splitting of the excited state.

In the spectra that is obtained, the doppler free signal can be seen as reduced absorption for the probe beam. There will also be cross over signals between all of the levels in the excited state. Altogether it is possible to see six sub-Doppler structures.

The six sub-Doppler structures arise when the pump and probe beams communicate with the same atoms. Three of the structures are located at the transition frequencies. At these positions the pump and probe interact with atoms that that has no velocity component parallel to the beams. The other three features are cross over signals. They come from atoms that have doppler shifts that make them resonant with both pump and probe, but at different transitions. The transitions have the same ground state but different excited states. A more detailed discussion can be found in [21].

If there would have been only one ground state to which the atoms could deexcite the crossover signals would be much weaker than the doppler free signals that are at the transition frequencies. In rubidium there are two possible ground states to which the atoms can deexcite. All of the sub doppler structures except for the closed transitions will get broader and deeper due to optical pumping processes. The pump not only saturates the transition, it also pumps away the atoms to another ground state, which significantly decrease the absorption for the pump beam. It takes very few photons to pump away atoms, that is why there is reduced absorption in a wide area by the sub doppler structures. It is important to identify all the sub doppler structures to be able to lock the laser to the right transition [21]. In figure 3.10 a theoretical saturation spectrum is shown.

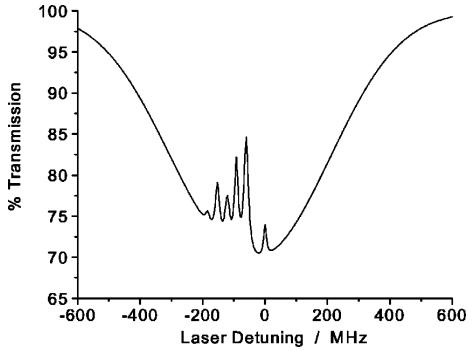

Figure 3.10: Sub-doppler spectrum for ^{85}Rb. The horizontal axis is the laser detuning relative to the cooling transition, $F_a = 3 \rightarrow F_b = 4$.
The six sub-Doppler features are from left to right, $F_a = 3 \rightarrow F_b = 2$, a crossover resonance ($F_a = 3 \rightarrow F_b = 2, 3$), $F_a = 3 \rightarrow F_b = 3$, a cross over resonance($F_a = 3 \rightarrow F_b = 2, 4$), a crossover resonance($F_a = 3 \rightarrow F_b = 3, 4$) and $F_a = 3 \rightarrow F_b = 4$. The spectrum of ^{87}Rb look similar. [21]

Chapter 4

The laser system

4.1 The laser diode

4.1.1 Light Emitting Diodes

The energy levels in a semiconductor are basically two bands of very close lying levels, the valence band and the conduction band. The two bands are separated by a band gap where no energy levels are present. A pure semiconductor is an isolator, with no free charge carriers. By injecting a donor material (n) free electrons are produced in the conduction band. If accceptors (p) are injected free holes (missing electrons) are produced in the valence band.

A light emitting diode (LED) can be constructed out of a pn-junction, just like a plain diode used in electronic circuits. One side of the diode is p-doped and the other is n-doped. These parts are separated by a depletion region. The p- and n-regions are not charged, but they are conductors due to free electrons (n-type) and free holes (p-type). In the depletion region the free electrons from the n-type material have recombined with holes from the p-side.

Electrons that have left the n-side of the depletion region make that part of the depletion region positively charged and the holes that have left the p-side of the depletion region make that side negatively charged. The negatively and positively charged regions lead to a varying electric potential in the depletion region.

The varying potential results in a distribution of electrons and holes as shown in figure 4.1 a. When applying a forward bias voltage the electrons and holes can diffuse into and across the depletion region [5]. When the electrons and holes recombine photons are emitted, as shown in figure 4.1 b. Plain diodes are constructed to avoid recombination in the depletion region. In LED:s on the other hand it is desirable.

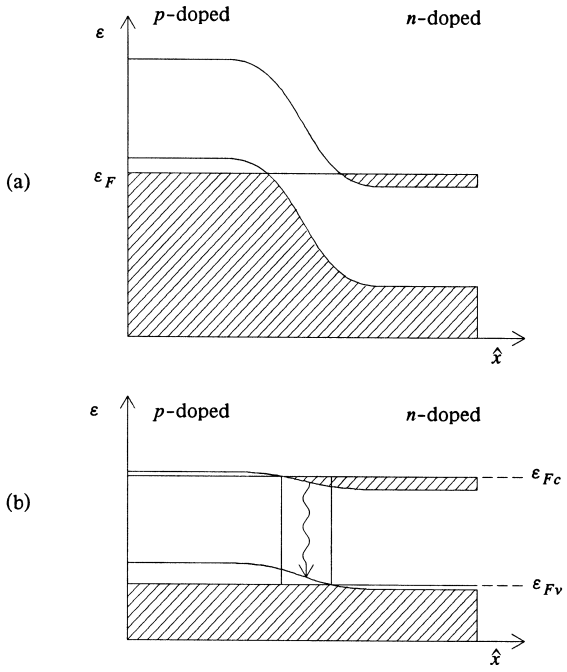

Figure 4.1: (a)A pn-junction with its built in potential. Dashed areas illustrate energy levels that are occupied with electrons. (b) A forward biased pn-junction with recombination in the depletion region. [6]

4.1.2 Semiconductor lasers

The simplest kind of diode laser is the homostructure laser diode, based on a single pn-junction. They were first realized, in 1962 [6]. Homojunction diodes can only emit a continuous wave at very low temperatures. Today the more complicated heterostructure diodes made by several layers of semiconductor materials have replaced the homojunction laser. The basic principles of a semiconductor laser are however easier to present in the case of the homojunction laser.

The active region of the homostructure laser diode is the pn-junction. The difference from a LED is that the junction is placed inside an optical resonator. A simple way of doing this is to polish the ends of the material in which the pn-junction is embedded. The junction will act as a waveguide due to differences in refractive index of the junction and surrounding semiconductor material. The polished ends will act like mirrors with a reflectivity of around 0,3 [6].

To produce coherent laser light stimulated emission must dominate over spontaneous emission. Light amplification in the pn-junction implies population inversion in the junction. There is a very well defined limit when stimulated emission become dominant in a laser diode. When the junction is forward biased with a voltage that lets a current I_{th} through the diode, it is on the threshold of lasering. With less current through the diode it works as a LED. Above threshold the junction is pumped fast enough for laser action to take place.

When electrons and holes recombine spontaneously, the emitted light has a wavelength spread that is quite big, ∼20 nm [16]. This is the gain profile of the active layer in the diode laser. The feedback in the laser cavity requires lasing at a wavelength where a standing wave can form in the cavity.

$$f_{cavity} = n\frac{c}{2L_{optical}} \tag{4.1}$$

n is an integer and $L_{optical} = n_{ref}L$. n_{ref} is the refractive index of the semiconductor. Light will be emitted at the frequencies of one (single mode laser) or a few (multi mode laser) cavity modes. The diode that has been used in this project is a single mode diode, Sanyo DL-7140-201. The following section implies a single mode laser.

The wavelength of the diode laser can be adjusted by changing the temperature of the laser or the current through it. Increasing the temperature and the current both tends to increase the central wavelength of the gain profile. The optical length of the cavity also gets larger, when the same parameters are increased.

When increasing the temperature the gain profile moves faster than the cavity mode. Laser action will always be at the wavelength with smallest losses. When the center of the gain profile moves away from the lasing cavity mode, another mode become more centrally located, the laser will then jump to the next cavity mode. Between the mode jumps the wavelength changes ∼0.06 nm/K. With the mode jumps included the average wavelength displacement is ∼0.3 nm/K [12]. When varying the current the wavelength shifts are very small compared to the shifts due to temperature changes. The relationship between gain profile displacement and cavity mode displacement is a little different compared to the

temperature induced changes. When varying both current and temperature it is possible to cover a little part of each wavelength gap that occur when only varying the temperature. The gain profile moves faster than the cavity modes even when adjusting the current and it is however not possible to cover all wavelengths.

4.1.3 Laser diodes at 780 nm

A laser diode based on AlGaAs can be made with its gain peak at 780 nm. The refractive index of an AlGaAs laser is about 4. It depends on the charge carrier distribution, i e the current through the active region. The cavity length of a diode laser is usually around 0,25 mm [6]. The optical length is then 1 mm. from equation 4.1 it can be seen that the frequency difference between consecutive cavity modes is:

$$\Delta f_{cavity} = \frac{c}{2L_{optical}} \approx 150\ GHz \tag{4.2}$$

The linewidth obtained by only accounting for the cavity losses is about 60 GHz, assuming uncoated facets (R$\approx$ 0.3). This is about a 1000 times the actual line width of a typical diode laser.

When also taking the gain in the cavity into consideration, the photon lifetime in the cavity increases [14].

$$\tau_{cavity} = -\frac{2L_{optical}}{c(\gamma - G)} \tag{4.3}$$

The corresponding linewidth $\delta f_{cavity} = 1/(2\pi\tau_{cavity})$ is typically 1 MHz. However there are broadening effects such as, variations in the refractive index, phase and intensity fluctuations due to spontaneous emission which lead to an enhanced linewidth, $\delta f_{enhanced} \approx 100$ MHz.

In high power laser diodes the back surface is often reflection coated and the front surface is anti reflection coated. The gain in the active layer is higher than in low power diodes. The obtained linewidth is not very different from a diode with two uncoated ends. The diode that was used in the constructed system is a high power diode, rated to deliver 80 mW.

The beam that leaves the laser diode is divergent. The divergence of the used diode is $\theta_{\perp} = 17^{\circ}$ and $\theta_{//} = 7^{\circ}$. $\perp$ denotes the divergence perpendicular to the polarization direction and // parallel to the polarization.

4.2 Littrow configuration external cavities

To make the diode laser more tunable without mode jumps and to narrow the emission linewidth of the laser, external cavities with frequency selective feedback are often used. External cavity diode lasers are also more stable and suitable to lock at a precise frequency. In this project a Littrow designed external cavity was used for this purpose.

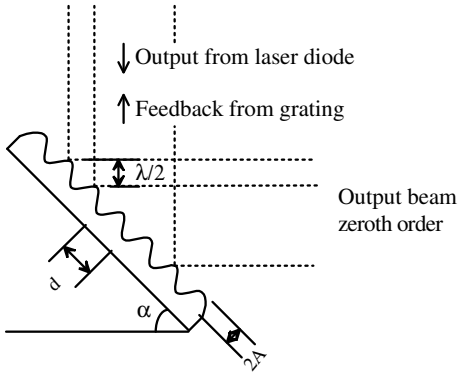

Figure 4.2: Littrow feedback mount.

4.2.1 Grating feedback in extended cavities

In a Littrow configuration external cavity diode laser, frequency selective feedback to the laser diode is provided by a diffraction grating, as shown in figure 4.2. Before being diffracted by the grating, the divergent light from the laser diode is collimated by a lens. The minus first order is coupled back into the laser diode and the zeroth order reflection is the outcoupling from the cavity. The zeroth order is the direct reflection. When coupling back the minus first order the following relationship must be fulfilled to get positive interference of the back coupled light.

$$d \sin \alpha = \frac{\lambda}{2} \tag{4.4}$$

At 780 nm, using a grating with a groove frequency of 1800 lines/mm, the angle of the grating (α) must be 44.6°.

To maintain a high reflectivity at 780 nm a gold coated grating is preferable. Holographic gratings are widely used in this type of applications[13][15][18][19]. The grooves on a holographic grating are created by exposing a holographic film by a standing wave pattern from lasers. This way the grooves get a sinusoidal shape. The reflectivity and the modulation depth of the grating decide how much light that is coupled back into the cavity. The modulation depth is denoted A in figure 4.2. The grating used in our cavity is manufactured by Richardson Grating Laboratory and has part number, 33999FL02-330H. The part number denotes all the parameters of the grating. This type of grating has a feedback of 20% to the diode[13].

The frequency width of the feed back to the laser depends on how many groves that are irradiated. The resolution of a grating is $R = N \cdot m$ [17]. N is the number of irradiated grooves and m is the diffraction order. In the cavity constructed in this work, m=(-)1. To find out the number of irradiated grooves the divergence of the beam from the diode and the focal length of the collimating lens (Thorlabs C230TM-B) are used. The used grating works best when the polarization is parallel to the grooves. The beam width perpendicular to the grooves is $d_\perp = 2l_{focal} \tan \theta_\perp$=2,8 mm. The beam hits the grating at a 45°

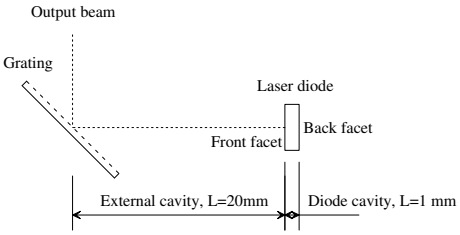

Figure 4.3: The extended the diode cavities.

angle. The number of irradiated grooves is, $N = f_{groove} d_{\perp} / \cos 45^{\circ} = 7000$. f_{groove} is the number of grooves per mm. The linewidth of the feedback to the laser diode is [17],

$$\delta f = \frac{f_{laser}}{N} \approx 55\ GHz \tag{4.5}$$

In this design the length of the Littrow cavity is 20 mm. The spacing between standing waves in this cavity is,

$$\Delta f_{Littrowcavity} = \frac{c}{2L_{optical}} \approx 7.5\ GHz \tag{4.6}$$

The increased cavity length compared to the diode, combined with a good mechanical stability of the mirror mount reduces the linewidth considerably. A linewidth of 370 kHz has been reported on the type of laser that has been constructed [15]. This narrow linewidth implies high quality current and temperature controllers.

No matter what type of laser it always tends to lase where the losses are as small as possible. When trying to control the frequency of a diode laser by placing it in an external cavity with frequency selective feedback, the lowest losses must be at the desired frequency.

If the front facet of the diode laser is anti reflection coated, a cavity is created between the back facet of the diode laser and the grating, see figure 4.3. To get laser action the losses must be smaller than the gain. The gain profile can be moved by changing the temperature of the diode to place the center of the gain profile closer to the desired lasing wavelength. The angle of the grating selects one of the cavity modes where the laser will lase.

The laser used in this design has a partly antireflection coated front facet. The cavity of the diode is still present and a compound cavity is formed. To minimize the losses at the frequency of the external cavity mode selected by the grating two conditions have to be fulfilled. As in the description above for anti reflection coated diodes, the gain curve has to be moved to place its center close to the desired lasing wavelength. In addition to that one of the diode cavity modes has to be placed at the frequency of the external cavity mode that is selected by the grating. If this is not done, the losses might be smaller when the diode is lasing in the short cavity mode that is in the center of the gain profile.

There is some tunability even if the diode is not antireflection coated. The laser

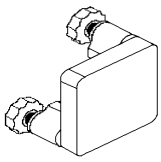

Figure 4.4: A Newport mirror mount with unmodified front plate.

will follow the external cavity, even if the external cavity forces the diode to lase at a wavelength that is a little displaced from the internal cavity mode, as long as the losses are lower when lasing at the external cavity wavelength. To get improved tunability the current through the laser can be varied during the sweep [16]. The tunability of the laser is not the most important property of a laser system used for cooling and trapping, as the laser shall be locked to an atomic transition, stability is much more important.

4.3 Design

The design of the constructed external cavity is described in two articles. The first one was written by A. S. Arnold, J. S. Wilson and M. G. Boshier in 1998 [13]. The second one written by C. J. Hawthorn, K. P. Weber and R. E. Scholten [15] is a development of the first design with some improvements, the biggest difference is an added mirror to get a fixed direction output beam. The constructed lasers have some different solutions compared to the designs in the articles, but the performance ought to be similar.

4.3.1 The cavity

The external cavity is constructed around a mirror mount. The mirror mount that was used can be seen in figure 4.4. This type of mount is mechanically stable and the angle and position of the front plate can be adjusted.

The front plate was modified to act as mount for the grating and a mirror that keeps the output direction of the beam constant. The mirror is a dielectric Near Infra Red mirror from Thorlabs. A large section of the front plate was machined away according to the drawing in figure 4.5. The grating is not mounted directly onto the modified front plate but on a small aluminium grating holder, figure 4.6, that is fixed onto the front plate by screws.

The length of the external cavity and the grating angle can be adjusted manually by the differential adjustment screws. When these screws are locked from coarse to fine adjustment they have two builtin threads working in opposite direction. The pitch of the two threads differ a little. When turning the knob one lap, the net displacement of the screws ball end is the difference of the displacement of

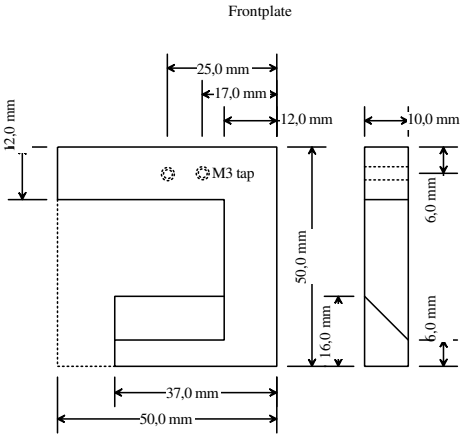

Figure 4.5: Drawing of the modified frontplate.

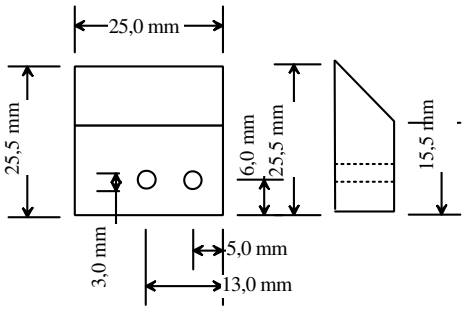

Figure 4.6: Drawing of the grating holder.

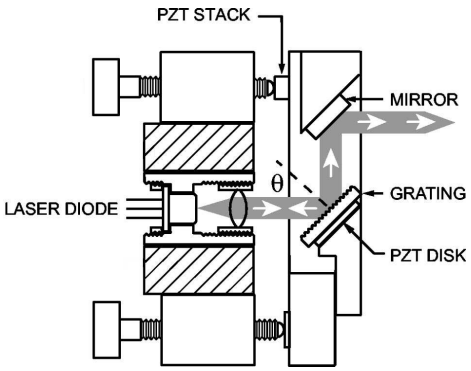

Figure 4.7: A cross section of the external cavity diode laser.
[15]

the two threads.

For even finer adjustment of the cavity length and grating angle there are two piezo electric transducers. In between the grating and the grating holder there is a small piezo disk. This disk is used to vary the cavity length. The disk has a quite low displacement per applied volt. Underneath the ball head of one of the fine adjustment screws a piezo stack is placed. It must be placed under the screw that changes the cavity length and angle but not the alignment of the cavity. The piezo stack has a higher displacement sensitivity than the disk.

The mirror mount is fixed to an aluminium base plate by screws. On this plate a temperature transducer (AD590) is mounted. When applying between 4 V and 30 V to the transducer the current through the transducer changes with the surrounding temperature, 1μA/K. This current acts as feedback to a temperature controller. The temperature controller can change the temperature of the external cavity by a peltier element able to both cool and heat. The Peltier element is clamped between the base plate and a big aluminium block that acts as a stand and a heat sink.

A cross section of the external cavity laser can be seen in figure 4.7.

The Peltier elements were chosen to fit temperature controllers based on a module from Wavelength Electronics, HTC3000. The Peltier elements were purchased from Supercool, their cooling power is 20W at a voltage of 9,2 V and a current of 3,9A. They will not reach maximum power as the gain of the controllers is decreased to avoid oscillations in temperature. The maximum output voltage is less than 2 V.

To avoid fluctuations in the laser temperature, a cover to protect the laser from draughts was constructed.

The current through the laser diode is controlled by a commercial diode laser driver, Melles Griot 06DLD201.

4.4 Adjusting the laser

In order to get the grating feedback into the laser diode, the external cavity has to be aligned. This can be done by observing the beam on an infra red viewing card. If there is an additional spot outside the main beam the cavity is not aligned. The additional spot is the diffracted beam that is supposed to be fed back into the diode that gets reflected. By turning the adjustment screws on the mirror mount the additional beam can be moved to coincide with the main beam. When this is done correctly, the output wavelength can be changed by turning the adjuster that changes the grating angle and cavity length. To monitor the change a wavelength meter is needed.

When the diodes are used in free run, they have an output wavelength of approximately 783 nm, at a temperature of 25°C. To move the gain profile closer to the D2 line of rubidium at 780,23 nm, the diode has to be cooled. As mentioned in section 4.1.2, the peak of the gain profile moves about 0,3 nm/K when changing the temperature of the diode. This means the diode has to be cooled from 25°C to 15°C. At this temperature condensation of water from the air starts to become a problem. To minimize this problem the cover must be kept on the laser as much as possible. When the cover is on, the amount of moisture that can condensate is limited.

Once the diode is cooled, the grating angle can be adjusted to get feedback at the desired wavelength. If it is not possible to get any output at 780,23 nm, that wavelength is probably in the middle of two diode cavity modes. By changing the current through the diode slightly this can be corrected.

4.5 Stability and tunability

A stable temperature is very important to avoid that the frequency of the laser starts to drift. With the cover mounted on the laser, it seems stable when performing saturation spectroscopy. When locking the laser slightly detuned from the cooling transition the demands are higher, but the frequency locking electronics will assist.

The external cavity length can be tuned by applying a voltage on the piezo disk or the piezo plate. A voltage of 15 volts applied on the disk changes the output frequency by 50 MHz. The piezo stack is more sensitive, 15 volts on the stack changes the frequency by 300MHz. It takes high voltages to perform long wavelength scans with the disk.

When saturation spectroscopy was performed the piezo stack was used to tune the frequency. It has to be evaluated which of the transducer will work best for locking the frequency. Both of them can be used simultaneously with different voltage amplitudes to make the grating turn around the pivot point while regulating.

The central wavelength of the grating feedback and the external cavity mode

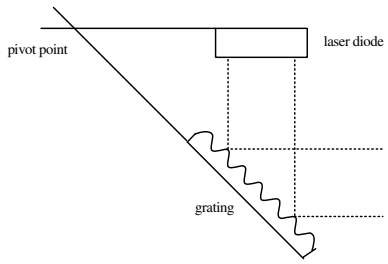

Figure 4.8: Mode jump free tuning of the output wavelength can be done by turning the grating around the pivot point.

are tuned by the same amount when the grating is turned around the pivot point, see figure 4.8. By tuning this way mode jumps between external cavity modes are eliminated.

4.6 Lock in amplifier circuit

The lock in amplifier design and two circuit boards are received from Anders Kastberg, University of Umeå. Two advanced lock in amplifiers have been constructed in our electronics workshop. the amplifiers are not yet tested.

The circuit regulates the frequency lasers to keep them on the cooling transition and hyperfine pumping transition.

The lock in circuits receive their signal from photodiodes in the saturation spectroscopy setup. The circuits contain oscillators to modulate the piezo transducers and thereby the output frequency of the lasers for lock in detection.

To be able to tune the frequency to find the transitions there is also a ramp function included. When the cooling transition or hyperfine pumping transition is found, the circuit regulates the piezos to maintain the right frequency.

Chapter 5

Conclusions

In summary, we have presented a design of a low-cost and simple MOT. The project has costed about 25000 SEK so far. The total cost will probably be less than 50000 SEK.

The project was not very well defined in the in the beginning. The initial project to construct optical molasses was changed to designing a MOT. The simplicity of the pyramidal MOT was very appealing, and it was decided to go for that design.

The diode lasers that initially were planned to be used are replaced by two external cavity diode lasers, with much better performance. They exhibit a more narrow linewidth and can be locked to an atomic transition with higher precision. Assisting electronics to stabilize the output frequency have also been built.

Most of the parts that are needed to construct the pyramidal MOT are purchased or constructed. There is however work left before cold rubidium atoms can be studied in Lund. There will be another Master's project to get the designed MOT realized.

Acknowledgements

Many people have shared their knowledge, time and equipment during this project. I would like to thank the following people for contributing:

My supervisor Prof. Anne L'Huillier,

Prof Anders Kastberg, especially for the lock-in circuit boards,

Prof Sune Svanberg,

Dr. Janis Alnis,

Åke Bergquist,

Dr. Sebastien Sauge,

The Photon Echo group, mainly Lars Rippe and Prof. Stefan Kröll.

The Diode Laser Spectroscopy group, particularly Gabriel Somesfalean and Linda Persson.

Bibliography

[1] H. J. Metcalf and P. van der Straten, *Laser Cooling and Trapping*, Springer-Verlag, 1999.

[2] O. Svelto, *Principles of Lasers*, Kluwer Academic/Plenum Publishers, 1998.

[3] B. H. Brandsen and C. J. Joachain, *Physics of Atoms and Molecules*, Longman Group Limited, 1983.

[4] P. A. Tipler, *Physics for Scientists and Engineers*,W. H. Freeman and Company, 1999.

[5] Günter Grossman,*Semiconductor Physics*, Lund Institute of Technology, 2003.

[6] W. W. Chow, S. W. Koch and M. Sargent III, *Semiconductor-Laser Physics*, Springer-Verlag, 1994.

[7] K. I. Lee, J. A. Kim, H. R. Noh and W. Jhe, *Single-beam atom trap in a pyramidal and conical hollow mirror*, Optical Letters 21, 1177-1179, 1996.

[8] A. Kastberg,*Laserkylning och Bose-Einstein-kondensation*, Kosmos, 31-36, 1996.

[9] C. Wieman, G. Flowers and S. Gilbert, *Inexpensive laser cooling and trapping experiment for undergraduate laboratories*, American Journal of Physics 63, 317-330, 1994.

[10] A. S. Mellish and A. C. Wilson, *A simple laser cooling and trapping apparatus for undergraduate laboratories*, American Journal of Physics 70, 965-971, 2002.

[11] SAES Getters, *Alkali Metal Dispensers*

[12] Lars Engström, *Atomfysik F3 2002*, KFS i Lund AB, 2002.

[13] A. S. Arnold, J. S. Wilson and M. G. Boshier, *A simple extended-cavity diode laser*, Review of Scientific Instruments 69, 1236-1239, 1998.

[14] C. H. Henry, *Theory of the Linewidth of Semiconductor Lasers*, IEEE Journal of Quantum Electronics 18, 259-264, 1982.

[15] C. J. Hawthorn, K. P. Weber and M. G. Boshier, *Littrow configuration tunable external cavity diode laser with fixed direction output beam*, Review of Scientific Instruments 69, 2001.

[16] T. Nayuki, T Fujii, K. Nemoto, M. Kozuma, M. Kourogi and M. Ohtsu, *Continuous Wavelength Sweep of External Cavity 630 nm Laser Diode without Antireflection Coating on Output Facet*, Optical Review 5, 267-270, 1998.

[17] S. Svanberg, *Atomic and Molecular Spectroscopy*, Springer-Verlag, 2001.

[18] J. J. Maki, N. S. Champbell, C. M. Grande, R. P. Knorpp and D. H. McIntyre, *Stabilized diode-laser system with grating feedback and frequency-offset locking*, Optics Communications 102, 251-256,1993.

[19] G. Genty, A. Gröhn, H. Talvitie, M. Kaivola and H. Ludvigsen, *Analysis of the Linewidth of a Grating-feedback GaAlAs Laser*, IEEE Journal of Quantum Electronics 36, 1193-1198, 2000.

[20] D. A. Steck, *Rubidium 87 D Line Data* Los Alamos National Laboratory, 2001.

[21] D. A. Smith and I. G. Hughes, *The role of hyperfine pumping in multilevel systems exhibiting saturated absorption*, American Journal of Physics 72, 631-637, 2004.

Appendix A

Laboratory exercise